Laser Spectroscopy on Forbidden Transitions in Trapped Highly Charged Ar^{13+} Ions

V. Mäckel,* R. Klawitter, G. Brenner, J. R. Crespo López-Urrutia, and J. Ullrich

Max-Planck-Institut für Kernphysik, Saupfercheckweg 1, 69117 Heidelberg, Germany

(Received 16 July 2011; published 27 September 2011; corrected 8 February 2012)

We demonstrate resonant fluorescence laser spectroscopy in highly charged ions (HCI) stored in an electron beam ion trap by investigating the dipole-forbidden $1s^2 2s^2 2p\ ^2P_{3/2}$–$^2P_{1/2}$ transition in boronlike Ar^{13+} ions. Forced evaporative cooling yielded a high resolving power, resulting in an accurate wavelength determination to $\lambda = 441.255\,68(26)$ nm. By applying stronger cooling and two-photon excitation, new optical frequency standards based upon ultrastable transitions in such HCI could be realized in the future, e.g., for the search of time variations of the fine-structure constant.

DOI: 10.1103/PhysRevLett.107.143002 PACS numbers: 32.10.Fn, 32.30.Jc, 32.60.+i, 95.30.Dr

Highly charged ions (HCI) are ubiquitous. Precise knowledge of their spectra is indispensable for the interpretation of astronomical observations, as well as for the diagnostics of laboratory plasmas. Thus, optical (*coronal*) lines [1] arising from electric dipole (E1) forbidden transitions in HCI allow for temperature and density determinations in the solar corona. Such transitions, often of magnetic dipole (M1) character, proceed between fine-structure levels basically resulting from relativistic effects. Moreover, they contain large quantum electrodynamic (QED) contributions. Their investigation allows for testing relativistic electron correlations [2] in systems with only few bound electrons. In principle, excellent accuracy can be obtained, since the strong nuclear Coulomb field reduces the polarizability of the optical electron roughly with the atomic number Z by Z^{-4} [3]. In addition, the fine-structure splitting by far dominates over the Zeeman splitting, and the central wavelength is unaffected by magnetic fields. Therefore, the sensitivity of the transition energy of such forbidden lines in HCI to external fields, e.g., lasers or blackbody radiation, is reduced by orders of magnitude. Ultimately, this inherent stability may prove important for the realization of novel laser frequency standards.

Accessibility of these lines by visible lasers is very advantageous. In contrast, electric dipole allowed (E1) transitions in HCI generally lie in the VUV and x-ray regions. While those can now be directly explored using free-electron lasers [4], measurements reach relative accuracy of only 300 ppm due to both insufficient resolution and means of absolute calibration. Unfortunately, three-level and electron-shelving schemes usually applied for the detection of forbidden transitions in atoms and ions of low charge cannot be easily transferred to HCI, since E1 transitions connecting metastable levels to fast decaying ones lie well beyond the optical range. Thus, resonant laser spectroscopy (RLS) has to proceed in a two-level scheme, with both extremely small excitation and decay rates. Nonetheless, RLS on forbidden transitions in HCI has already been reported for relativistic hydrogenlike Bi^{82+} [5] and Pb^{81+} [6]. Here, ion momentum uncertainty translates into Doppler shifts of 100 ppm relative accuracy. Proposed setups using co- and counterpropagating laser beams (see, e.g., [7]) could alleviate these problems. However, it is clear that only by using trapped and cooled HCIs a precision similar to that achieved nowadays in atoms [8,9] and ions in low charge states [10] can be reached for HCI. Decelerating the HCI produced at about 50% of the speed of light down to rest, as planned in the HITRAP facility [11] is a still unsolved challenge.

Here we report on RLS of the $1s^2 2s^2 2p\ ^2P_{3/2}$–$^2P_{1/2}$ transition in B-like Ar^{13+} at the electron beam ion trap (EBIT) [12] at the Max-Planck-Institut für Kernphysik in Heidelberg. We apply a singe photon excitation scheme and monitor directly the decay of the excited $1s^2 2s^2 2p\ ^2P_{3/2}$ metastable level with a lifetime of 9.573 ms [13]. Excellent accuracy ($\delta\lambda/\lambda = 0.6$ ppm) has been achieved by forced evaporative cooling, challenging the most precise conventional spectroscopy measurements and opening the path towards ultraprecise RLS in HCI. The experimental arrangement is shown in Fig. 1.

An EBIT is well suited for these spectroscopic investigations, since its monoenergetic electron beam selectively strips atoms to any desired ionic charge state [14], up to hydrogenlike [15] uranium, at rest. Collisional quenching of metastable states can be made negligible. Even when the electron beam is switched off, in the so-called magnetic trapping mode [16], EBITs still operate like a Malmberg-Penning trap [17], thus avoiding transfer losses between ion source and trap.

Early proposals made for RLS at the Oxford EBIT aimed, e.g., at exciting the M1 transition in Be-like Ar^{14+} [18] or driving the $^2S_{1/2}$-$^2P_{3/2}$ transition in hydrogenlike Si^{13+} [19]. The first successful experiment was the excitation of the $^2S_{1/2}$-$^2P_{3/2}$ transition in hydrogenlike N^{6+} by monitoring the enhancement of the Lyman-α emission induced by the laser radiation [20]. As the upper level is naturally broad, the achievable relative accuracy was severely limited to only 600 ppm.

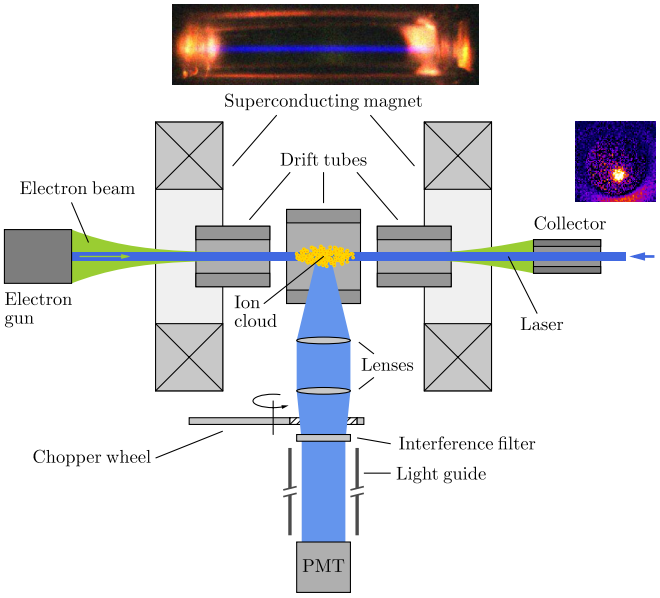

FIG. 1 (color online). Scheme of the setup. An electron beam compressed by a coaxial 8 T magnetic field produces Ar^{13+} ions by electron impact and traps them subsequently. The ions are irradiated by a coaxially superimposed tunable laser, and their resonant fluorescence observed with a photomultiplier. Top: Collisionally excited forbidden line emission of the cloud of trapped Ar^{13+} ions, side view. Right: End-on view though the collector.

An EBIT uses a highly compressed electron beam to both ionize and trap ions. It is produced by a thermionic cathode biased to a negative potential and accelerated towards a trap consisting of a series of drift tubes. Thereby it is compressed at the trap center to a radius below 50 μm by means of a strong magnetic field of 8 T generated by superconducting Helmholtz coils. After passing the trap, the now again expanding electron beam is decelerated, and then dumped on to a water-cooled collector. A tenuous ballistic Ar atomic beam is continuously injected through a differentially pumped system, crossing the electron beam at the trap center. There, ions are produced by sequential electron impact ionization. They are trapped radially by the negative space charge of the beam, but also by the magnetic field. Axial trapping is provided by positive potentials applied to the drift tubes before and after the trap center. The ion motion is thus confined to a cylindrical volume with a diameter of ca. 500 μm and a length of 40 mm, centered around the electron beam. The position and the size of the Ar^{13+} ion cloud inside the trap are determined by imaging the photons of the M1 emission line (due to collisional excitation) through the collector onto an intensified CCD camera. An (uncorrected for the apparative width) full-width-at-half-maximum (FWHM) of its projection is 580(30) μm, similar to findings at the NIST EBIT [21]. Additionally, a side view image of the ion cloud was recorded using a conventional CCD camera (Fig. 1 upper part).

The magnetic field splits the M1-transition into six line components. As this energy splitting is very small compared to the fine structure, which is in this case basically identical to the transition energy, they appear in a symmetrical pattern, consisting of four outer π (two π^- and two π^+) and two inner σ transitions [22].

Excitation is performed by means of a pulsed Nd:YAG laser (Spectra-Physics GCR-190) running at 100 Hz, with a pulse duration of 9 ns, pumping a tunable dye laser (Sirah PrecisionScan) which yields a power up to 1.2 W at 440 nm with a linewidth of 1.2 Ghz. The linear polarized laser beam enters the EBIT through the collector axis (see Fig. 1) and is brought to overlap coaxially with the ion cloud. Approximately 10^{16} photons per pulse are focused down to ≈ 0.1 mm^2 at the trap center. Since the laser propagates parallelly to the magnetic field lines, only the four π components are excited. This configuration, nonetheless, guarantees for maximal overlap between the ion cloud and the laser.

For the detection of fluorescence photons two quartz lenses with a diameter of 38 mm and a focal length of 150 mm are installed inside the EBIT vacuum. They cover a solid angle of 0.05 sr and produce a real image of the ion cloud just outside the vacuum viewport on one side of the EBIT. At this position, the optical path is periodically blocked mechanically by a synchronized chopper wheel in order to eliminate stray light coming from the pulsed laser. To suppress remaining stray light from the cathode, a narrowband interference filter at 445 nm with a FWHM of 20 nm and a minimum transmission of 93% (Semrock FF01-445/20) for the Ar^{13+} spectral line is used. The photons are then guided through an inside-polished, 1.15 m long aluminum tube to a photomultiplier (Photonis XD2821) with a bialcali cathode having a quantum efficiency of 15% and a dark-count rate of 8 s^{-1}, sufficiently far away from the strong magnetic field of the EBIT. All in all, the total detection efficiency is 0.02%.

Since the electron beam also strongly excites the M1 transition line, the beam is switched off before the fluorescence signal due to the laser excitation is measured. We apply a cyclical measuring scheme (Fig. 2) similar to the one used for lifetime measurements in EBITs [23–27]. Each cycle begins with the electron beam turned on, producing ions, and resulting in a high photon count rate. Then, the beam is switched off, leaving the ions trapped in magnetic trapping mode, during which collisionally excited metastable states decay. The ions can then only be reexcited resonantly by the laser. In the upper right of Fig. 2, the time evolution of the fluorescence is displayed for the sum of 78 000 single laser shots with the laser on and off resonance. A lifetime of 9(2) ms can be inferred, in good agreement with the value of 9.573(9) ms reported by Lapierre *et al.* [13] for the metastable $^2P_{3/2}$ level. For a wavelength scan the laser is set to the start value. Then, one ion production and storage cycle is performed, during

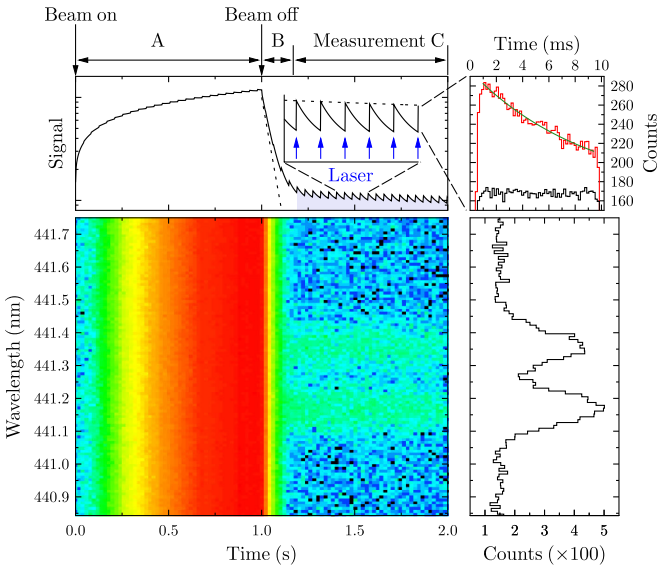

FIG. 2 (color online). Upper panel: Measurement cycle. (A) Ion production and excitation by the electron beam. (B) Beam is shut off; collisionally excited states decay. After five lifetimes, the projection area (C) starts. When the laser is in resonance, ions are excited by the laser pulses (indicated by the arrows) and decay again. Upper right: Decay (integrated over 78 000 pulses) of the fluorescence signal after a laser pulse; (red line): on resonance; (black line): off resonance. Lower left: Photon yield vs excitation wavelength during the cycle time. Right: Projection of the photon yield within the area (C).

which the wavelength stays constant. After this cycle the wavelength is incremented to the next value, and a new cycle is started. These cycles are repeated until the end of the scan is reached.

For simultaneous wavelength calibration, the optogalvanic effect of a Ne-filled hollow cathode lamp was used. Nine well known reference calibration lines from the NIST database [28] were taken for wavelength determination. Additionally, the interference pattern of an etalon with a free spectral range of 0.1 nm was monitored with a CCD camera at each wavelength step in order to provide additional, regular references. Each single scan was evaluated by fitting the wavelength scale with a least-squares algorithm to the line positions, thus obtaining the dispersion function. The accuracy of the calibration lines is of the order of 10^{-5} nm, with the total error being mainly caused by the statistical uncertainty of the peak position determination.

The photon yield as a function of the laser wavelength during a typical scan is shown in Fig. 2 (lower right panel). Time starts when the electron beam is switched on. For the projection onto the wavelength axis only the photons arriving later than five lifetimes after the electron beam is switched off are integrated, in order to let the collisionally excited states decay. All in all, four lines due to the Zeeman splitting are expected. However, first experiments showed that the individual Zeeman components could not be fully resolved due to the ion thermal Doppler broadening, but instead were visible as two maxima.

To improve resolution, forced evaporative cooling of the magnetically stored ions was applied. Often, cooling in an EBIT is done by using a reduced electron beam current with a lower space charge, and thus a shallow radial trapping potential. This also implies a reduction of the collisional heating rate, whereby ion temperatures as low as 6 eV have been reported [22]. Similarly, a low axial trapping potential can be used in order to enhance axial evaporative cooling [29]. For heavier ions, evaporative cooling is achieved by adding low-Z cooling gas [30]. While the ionization rate can be still kept high by maintaining a sufficiently high beam current [31], using a shallow trap however, reduces the number of trapped ions. Therefore, we use a new scheme by firstly producing ions, and then employing forced evaporative cooling during magnetic trapping mode. This was achieved by linearly lowering the axial potential governing the ion escape.

For the scans, B-like Ar^{13+} was produced for 1000 ms with an electron beam of 110 mA accelerated towards 1070 V, then the ions were kept in magnetic trapping mode for further 2000 ms for the first 26 scans. This period was extended to 3000 ms for the following 32 scans. During ion production the voltage of the drift tubes defining the axial potential was set to 200 V. Right after switching off the electron beam, it was linearly lowered to 20 V within 400 ms, thus increasing evaporative cooling, and then kept constant at 20 V. For a single wavelength scan the laser was tuned from 440.86 to 441.74 nm in steps of 1.1 pm.

Figure 3 shows the laser-induced fluorescence signal during the magnetic trapping mode. The data result from the accumulation of 58 single scans with a total acquisition time of 40 hours. Horizontal and vertical axes represent the laser wavelength and the ion trapping time after the electron beam is shut off, respectively. Just after turning off the electron beam, only two maxima are visible, which later evolve into resolved four Zeeman π components.

Assuming a Maxwellian distribution, the ion temperature T_i is given by

$$T_i = \frac{M_i c^2}{8 k_B \ln 2}\left(\frac{\Delta\lambda_d}{\lambda_0}\right)^2 \quad (1)$$

with M_i being the ion mass, c the speed of light, k_B the Boltzmann constant, λ_0 the central wavelength. Since other sources of broadening, like the natural linewidth of 6.5×10^{-11} nm and the laser bandwidth of 1.7×10^{-3} nm can be safely neglected, the ion temperature can be directly derived from the measured linewidth $\Delta\lambda_d$. The temperature development of the ions during and after cooling, which is derived from the mean linewidth of the four π transitions, is shown in Fig. 3 as red and white diamonds. While lowering the trap potential, the ion temperature, being initially 240 eV, follows the applied axial trap

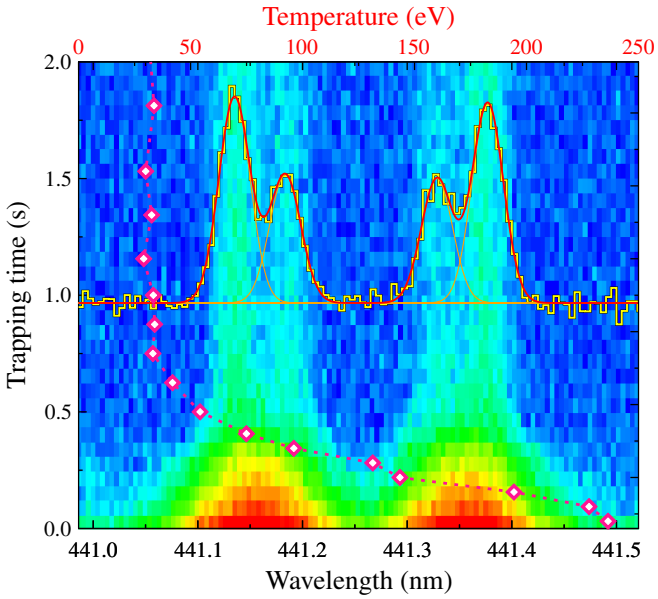

FIG. 3 (color online). Integrated fluorescence signal (blue: lowest; red: highest) with evaporative cooling in dependence of the trapping time and the laser wavelength. Also shown are the ion temperature evolution (red diamonds, upper scale) and the wavelength projection of the fluorescence signal after cooling, showing the four π components (from left to right: $\pi^{+}_{3/2}$, $\pi^{+}_{1/2}$, $\pi^{-}_{1/2}$ and $\pi^{-}_{3/2}$). Notice the rotation of this plot in relation to the one in Fig. 2.

potential V_{ax}, being around $0.01qeV_{\mathrm{ax}}$ (with q and e the ion an electron charge). The resolution has improved 700 ms after the beam is switched off to a linewidth of 28 pm, corresponding to an ion temperature of 28 eV, which reveals all Zeeman π components.

The projection of the signal onto the wavelength axis after cooling is also displayed in Fig. 3 (yellow histogram and red-line fit) using the data starting 700 ms after the beam is shut off until the end of the magnetic storage time. In order to obtain the central wavelength, groups of three successive scans have been summed up and their projections fitted using four Gaussians of the same width, with the additional condition that their splitting is symmetrical. Finally, the weighted mean has been derived, which yields 441.255 68(24) nm. The individual Zeeman components display a statistical uncertainty as small as 0.4 pm.

Taking into account the systematic uncertainties of the calibration lines of 0.00002 nm, a wavelength of 441.255 68(26) nm is obtained. This result perfectly confirms the measurement of Draganić *et al.* [32] yielding 441.2559(1) nm, and the value of 441.2556(1) nm determined by Soria Orts *et al.* [33], both performed using a conventional grating spectrometer. However, in contrast to those measurements, the current resolution is not limited by the instrument itself. Moreover, it is in excellent agreement with the best theoretical value of 441.261(70) nm [2], which still has an uncertainty that is larger by 2 orders of magnitude. As for now, theory can predict such lines only to a relative accuracy $\delta\lambda/\lambda$ of typically 1000 ppm, reaching only in exceptional cases the 100 ppm mark. Therefore, experiments are needed to validate and increase the knowledge of their wavelengths not only for applications in astrophysics, but also to improve atomic structure codes.

In conclusion, two-level RLS was demonstrated for a forbidden transition in trapped HCI, reaching excellent resolution by evaporative cooling. Cooling the ions inside the trap avoids any potential transfer losses. Moreover, this method can be used for probing the lifetime of metastable atomic levels.

Our present wavelength uncertainty is only 0.000 26 nm, which has to be compared with a QED shift of -0.96 nm [32], and a relativistic nuclear recoil isotope shift between ^{36}Ar and ^{40}Ar already on the order of 0.001 23(6) nm [33,34]. Studying forbidden optical lines with such large QED, nuclear size and recoil effects by means of RLS will significantly help our understanding of these fundamental interactions in the extreme regime of atomic physics found in HCI.

Higher accuracy shall be achievable by further ion cooling. In order to pursue this goal, we have constructed a cryogenic linear Paul trap for storing and sympathetically cooling HCI extracted from the EBIT. Retrapping and evaporative cooling of Ar^{18+} in a Penning trap has been recently reported [35]. Sympathetic laser cooling with indications of Coulomb crystallization was demonstrated by Gruber *et al.* [36] on Xe HCI, also in a Penning trap. Combining these approaches will open the exciting possibility of realizing precision optical frequency standards based upon forbidden transitions in HCI. Those, by virtue of their extremely low sensitivity to Stark and blackbody radiation shifts, might on the long run exhibit a frequency stability superior to that of any other atomic standards currently in use. Finally, as suggested recently, their large relativistic contributions makes them very sensitive tools to explore the possible temporal variation of the fine-structure constant [37,38].

*maeckel@mpi-hd.mpg.de

[1] B. Edlén, Z. Astrophys. **22**, 30 (1943).
[2] A. N. Artemyev *et al.*, Phys. Rev. Lett. **98**, 173004 (2007).
[3] J. D. Gillaspy, J. Phys. B **34**, R93 (2001).
[4] S. W. Epp *et al.*, Phys. Rev. Lett. **98**, 183001 (2007).
[5] I. Klaft *et al.*, Phys. Rev. Lett. **73**, 2425 (1994).
[6] P. Seelig *et al.*, Phys. Rev. Lett. **81**, 4824 (1998).
[7] J. K. Thompson, D. J. H. Howie, and E. G. Myers, Phys. Rev. A **57**, 180 (1998).
[8] T. W. Hänsch and H. Walther, Rev. Mod. Phys. **71**, S242 (1999).
[9] M. Niering *et al.*, Phys. Rev. Lett. **84**, 5496 (2000).
[10] T. Rosenband *et al.*, Science **319**, 1808 (2008).
[11] T. Beier *et al.*, Nucl. Instrum. Methods Phys. Res., Sect. B **235**, 473 (2005).

[12] J. R. Crespo López-Urrutia *et al.*, Phys. Scr. **T80**, 502 (1999).
[13] A. Lapierre *et al.*, Phys. Rev. Lett. **95**, 183001 (2005).
[14] M. A. Levine *et al.*, Phys. Scr. **T22**, 157 (1988).
[15] R. E. Marrs, S. R. Elliott, and D. A. Knapp, Phys. Rev. Lett. **72**, 4082 (1994).
[16] P. Beiersdorfer *et al.*, Rev. Sci. Instrum. **67**, 3818 (1996).
[17] J. H. Malmberg and C. F. Driscoll, Phys. Rev. Lett. **44**, 654 (1980).
[18] T. V. Back *et al.*, Hyperfine Interact. **114**, 203 (1998).
[19] A. Klein *et al.*, Lect. Notes Phys. **570**, 664 (2001).
[20] K. Hosaka *et al.*, Phys. Rev. A **69**, 011802 (2004).
[21] J. V. Porto *et al.*, Rev. Sci. Instrum. **71**, 3050 (2000).
[22] R. Soria Orts *et al.*, Phys. Rev. A **76**, 052501 (2007).
[23] F. G. Serpa *et al.*, Phys. Rev. A **55**, 4196 (1997).
[24] J. R. Crespo López-Urrutia, P. Beiersdorfer, and K. Widmann, Phys. Rev. A **74**, 012507 (2006).
[25] A. Lapierre *et al.*, Phys. Rev. A **73**, 052507 (2006).
[26] G. Brenner *et al.*, Phys. Rev. A **75**, 032504 (2007).
[27] G. Brenner *et al.*, Astrophys. J. **703**, 68 (2009).
[28] E. B. Saloman *et al.*, J. Phys. Chem. Ref. Data **33**, 1113 (2004).
[29] P. Beiersdorfer *et al.*, Phys. Rev. Lett. **77**, 5353 (1996).
[30] B. M. Penetrante *et al.*, Phys. Rev. A **43**, 4873 (1991).
[31] C. Beilmann *et al.*, Phys. Rev. A **80**, 050702 (2009).
[32] I. Draganić *et al.*, Phys. Rev. Lett. **91**, 183001 (2003).
[33] R. Soria Orts *et al.*, Phys. Rev. Lett. **97**, 103002 (2006).
[34] I. I. Tupitsyn *et al.*, Phys. Rev. A **68**, 022511 (2003).
[35] M. Hobein *et al.*, Phys. Rev. Lett. **106**, 013002 (2011).
[36] L. Gruber *et al.*, Phys. Rev. Lett. **86**, 636 (2001).
[37] J. C. Berengut, V. A. Dzuba, and V. V. Flambaum, Phys. Rev. Lett. **105**, 120801 (2010).
[38] J. C. Berengut *et al.*, Phys. Rev. Lett. **106**, 210802 (2011).